Available online at www.sciencedirect.com

jmr&t Journal of Materials Research and Technology

journal homepage: www.elsevier.com/locate/jmrt

Original Article

Different point defects originated from dissimilar deposition conditions in *n*-type Cu-doped Bi_2Te_3 films; crystal structure and thermoelectric property depending on Te-vacancy concentration

Byeong Geun Kim [a,1], *Kang Hyun Seo* [b,1], *Chang-Hyun Lim* [c], *Soon-Mok Choi* [b,*]

[a] *Research Development Division, Gyeongbuk Institute of IT Convergence Industry Technology, Gyeongsan-si, 38463, South Korea*

[b] *School of Energy, Materials and Chemical Engineering, Korea University of Technology and Education, Cheonan, 31253, South Korea*

[c] *Energy & Environmental Division, Korea Institute of Ceramic Engineering and Technology, Jinju, 52851, South Korea*

ARTICLE INFO

Article history:
Received 21 May 2021
Accepted 28 July 2021
Available online 14 August 2021

Keywords:
Thermoelectric
Bi2Te3
Defect
Doping

ABSTRACT

We found that two types of Cu-doped Bi_2Te_3 thin films fabricated by dissimilar sputter process had different microstructures and non-stoichiometries (Bi:Te ratios). We investigated the different levels of Te-vacancy (V_{Te}^{2+}) concentration in the films affected the point defects and the thermoelectric property of the films. The Cu additives were substituted for the Bi-sites (form Cu_{Bi}^{2-} defects) in case of a low Te-vacancy concentration (V_{Te}^{2+}) in the Bi_2Te_3 thin film. In the high V_{Te}^{2+}-defect concentration case, the Cu_{Bi}^{2-}-formation reaction was thought to be inhibited and evidences for the Cu-additive intercalating into a van der Waals layer (a Cu_{vdW} defect) were detected. We examined the lattice parameter, the thermoelectric properties, and the carrier transport properties of the two types of thin films with the different Te-vacancy concentrations as evidences for the different point defect formation characteristics between them. The Te-vacancy (V_{Te}^{2+}) dependency of the point defects formation (Cu_{Bi}^{2-} or Cu_{vdW}) in this system can suggest the clue to control an atomic scale Cu-site in n-type Cu doped Bi_2Te_3 thin films.

1. Introduction

Dimensionless figure of merit, $ZT = \sigma S^2 T/\kappa$ is an evaluation index for a performance of thermoelectric materials, where σ is the electrical conductivity, S is the Seebeck coefficient, and κ is the thermal conductivity at a given absolute temperature T [1–3]. As can be expected from the equation, the high performance (ZT) of the thermoelectric materials can be obtained from the reduced thermal conductivity (κ) [4]. Many thermoelectric materials such as GeTe [5], PbTe [6,7], Bi_2Te_3 [8], and silicides [9] have been studied to improve the thermoelectric performance.

* Corresponding author.
E-mail address: smchoi@koreatech.ac.kr (S.-M. Choi).
[1] These authors contributed equally to this work.

https://doi.org/10.1016/j.jmrt.2021.07.147

Bi_2Te_3-based materials are the commercially advanced thermoelectric systems especially at around room temperature [10–18]. Increasing point defect concentration is an effective way to decrease thermal conductivity of the materials specially for high frequency region phonons [4]. Chen et al. reported a remarkable *ZT* value 1.4 at 473 K from nanostructuring researches [10,11]. It was 1.5 times higher than the values from a zone melting process [10,11]. A Bi_2Te_3 material has a rhombohedral crystal structure having a quintuple layers with the order of layers $-Te^{(1)}$-Bi-$Te^{(2)}$-Bi-$Te^{(1)}$- [12]. A cleavage tends to occur in the lamellar-structured single crystal with weak van der Waals bond (vdW) between the two quintets [12]. The crack propagates along their basal planes, perpendicular to the c–axis resultantly [12]. The nanostructuring process has an additional advantage that it overcomes the poor mechanical properties of the zone melting specimens [12].

The nanostructuring approaches were reported to be especially available only for *p*-type Bi_2Te_3 materials because a formation of uncontrollable point defects including Te vacancy (V_{Te}^{2+}) provide causes of a reproducibility issue in the *n*-type $Bi_2Te(Se)_3$ systems [12]. Liu et al. reported that Cu additive atoms could improve the reproducibility of the *n*-type $Bi_2Te(Se)_3$ systems with V_{Te}^{2+} defects [12]. In addition, a high *ZT* value 0.99 at 400 K reported in the system was ascribed to the Cu-additive effect reducing thermal conductivity [12]. The effects of a Cu-additive in an *n*-type $Bi_2Te(Se)_3$ system have been a major topic in research for higher property and reproducibility of the system. Cu-additives can produce Cu_{Bi}^{2-} substitution defects and/or can be intercalated into the vdW bonding layer (Cu_{vdW}).

The sputter deposition is widely used and suitable for preparing the nanostructured-semiconductor films with various dopants in electric/optical applications [19–26]. In this process, the materials sputtered from source targets are deposited as atoms or nanoparticles with very small size under ultra-high vacuum. This facilitates the foreign dopants uniformly add into matrix films, and the doping effect can be intensely investigated. In additions, the process parameters such as deposition temperature, working pressure, electric power on targets permit the facile preparation of the materials with the desired compositions, microstructures, and thickness *etc*. Among them, the deposition temperature is the most important factor for control of microstructure and electrical properties of the films [25].

In this study, we prepared two distinct types of Cu-doped Bi_2Te_3 thin films with different defect chemistry by setting process order of heat-treatment differently in direct current (DC)/radio frequency (RF) sputter process. One is sputtering with a simultaneous heat-treatment and the other is post annealing after sputtering at room temperature. In case of the films deposited at room temperature, the post annealing was performed due to improving crystallinity of films, while the films deposited at high temperature not. We compared two Bi_2Te_3 films made by distinct sputtering conditions based on their different concentrations of Te-vacancy (V_{Te}^{2+}) in them. In addition, we tried to find evidences the Cu additive location depends on Te-vacancy (V_{Te}^{2+}) concentrations in to the Bi_2Te_3 films.

2. Methods

2.1. *Preparation of Cu-doped Bi_2Te_3 thin films*

Cu-doped Bi_2Te_3 thin films were deposited by co-sputtering with Cu (99.999%, Kojundo Chemical Laboratory Co., Ltd.) and Bi_2Te_3 (99.999 %, Kojundo Chemical Laboratory Co., Ltd.) targets. The vacuum of chamber was extracted by rotary pump until 3.2×10^{-6} Torr, and adjusted at 3 mTorr by injection of Ar gas (99.999%) with 40 sccm (standard cubic centimeters per minute). The quantities of Cu doping were controlled by the RF power (0–8 W) on Cu target, while the DC power on Bi_2Te_3 target was fixed at 40 W. Si wafers with SiO_2 layer (300 nm thickness) was used as the substrates, and were cleaned by the sonication with acetone (99.999%, Sigma–Aldrich) and ethanol (99.999%, Sigma–Aldrich) solutions before deposition. For uniform deposition, the substrates were rotated at 20 rpm during the deposition process. We carried out both the deposition with a simultaneous heat-treatment (at 200 °C) and the post annealing (at 300 °C) after sputtering at room temperature. The thickness of all films was about 400 nm. The condition of the post annealing was at 300 °C for 10 min using a horizontal rocking furnace under Ar gas (99.999%) atmosphere.

2.2. *Characterization*

The microstructural, morphological and structural properties of Cu-doped Bi_2Te_3 thin films were analyzed by field emission scanning electron microscope (FESEM) (JSM-7500F, JEOL Ltd, Japan)/(CUBE 1000, EmCrafts, Korea) and X-ray diffraction (XRD) (Empyrean, PANalytical B. V, Netherlands). The Cu-Kα radiation with $\lambda = 0.154056$ nm and a scanning rate of 4°/min were adjusted for the XRD measurement. The compositions and chemical properties of Cu-doped Bi_2Te_3 thin films were determined by X-ray photoelectron spectroscopy (XPS, K-Alpha, Thermo Fisher Scientific, UK). In case of Cu-doped Bi_2Te_3 thin films deposited at RT, the XPS analyses were performed after thermal annealing at 300 °C for 10 min under Ar gas atmosphere. For XPS measurement, the Ar^+ plasma etching was performed to remove oxide layers at surface of films for 3 min. First, the whole compositions of Cu-doped Bi_2Te_3 thin films deposited at RT were analyzed after thermal annealing, and were $Cu_{0.00}Bi_{2.00}Te_{1.58}$, $Cu_{0.01}Bi_{2.00}Te_{1.68}$, $Cu_{0.03}Bi_{2.00}Te_{1.62}$, and $Cu_{0.28}Bi_{2.00}Te_{1.35}$ as a function of Cu contents. The samples were named "ACu-*atomic content of Cu*" as follows: $Cu_{0.00}Bi_{2.00}Te_{1.58}$ (ACu-0.0), $Cu_{0.01}Bi_{2.00}Te_{1.68}$ (ACu-0.2), $Cu_{0.03}Bi_{2.00}Te_{1.62}$ (ACu-0.8), and $Cu_{0.28}Bi_{2.00}Te_{1.35}$ (ACu-7.7). The compositions of Cu-doped Bi_2Te_3 thin films deposited at 200 °C were $Cu_{0.13}Bi_{2.00}Te_{2.50}$, $Cu_{0.38}Bi_{2.00}Te_{3.35}$, and $Cu_{0.41}Bi_{2.00}Te_{2.62}$. The samples were named "HCu-*atomic content of Cu*" as follows: $Cu_{0.13}Bi_{2.00}Te_{2.50}$ (HCu-2.7), $Cu_{0.38}Bi_{2.00}Te_{3.35}$ (HCu-6.7), and $Cu_{0.41}Bi_{2.00}Te_{2.62}$ (HCu-8.1).

3. Results and discussions

First, we analyzed the actual composition of the Bi_2Te_3 matrix of the thin films doped with Cu atoms.

Table 1 – Compositions of ACu- and HCu-films prepared with different preparation conditions.

	Cu (at.%)	Bi (at.%)	Te (at.%)	Bi:Te ratio
ACu-0.0	0.00	55.91	44.09	1:0.79
ACu-0.2	0.18	54.26	45.56	1:0.84
ACu-0.8	0.83	54.86	44.31	1:0.81
ACu-7.7	7.66	55.13	37.22	1:0.68
HCu-2.7	2.71	43.22	54.07	1:1.25
HCu-6.7	6.68	34.86	58.46	1:1.67
HCu-8.1	8.06	39.78	52.16	1:1.31

An XPS analysis was used to determine the compositions of the Cu-doped Bi_2Te_3 thin films as a function of Cu contents and deposition processes; aging (300 °C) and high temperature deposition (200 °C) (Table 1). In order to distinguish films easily and conveniently, the Bi_2Te_3 films doped with Cu were indexed as Cu contents and deposition processes: the films annealed at 300 °C after deposition at RT were named by ACu-films (ACu-0.0, ACu-0.2, ACu-0.8, and ACu-7.7), while the films deposited with heating at 200 °C in situ were indexed as HCu-2.7, HCu-6.7, and HCu-8.1 (HCu-films). Notably, the molar ratio of Bi to Te in ACu-0.0–ACu-7.7 was not consistent with those of Bi_2Te_3 source target (Bi:Te = 2:3). They showed the deficient of Te components (2:1.4 ~ 2:1.7). However, the molar ratio in the HCu-2.7–HCu-8.1 films was nearly consistent with those of Bi_2Te_3 source target.

In general, the compositions of deposited elements are well corresponded with those of source targets in a sputter process with alloy target at room temperature. When Bi_2Te_3 atoms (or clusters) are deposited on the surface of films during sputtering, they diffuse through the surface of films and the grains are formed in general. The activation energy for the diffusion is supplied from the thermal energy of deposition temperature, which is important for the crystallization of films with well-organized crystals [25]. However, in case of the ACu-films sputtered at room temperature, the activation energy for the diffusion of the deposited Bi_2Te_3 atoms (clusters) is not sufficient. The followed annealing at 300 °C for the deposited clusters with high surface area could not contribute to crystallization of the cluster and instead accelerated an evaporation of source components. Hence, Te atoms with high vapor pressure may be evaporated during thermal annealing at 300 °C. The Te evaporation creates a point defect (V_{Te}^{2+}) into the Bi_2Te_3 matrix.

Cu contents gradually increased in proportion to the applied power on Cu target in all films. The Cu contents in thin films were a little different between the ACu-films and the HCu-films although the same powers of targets were applied. The quantities of Cu element were slightly larger in the HCu-films than those of the ACu-films, which may be due to the different deposition steps.

Fig. 1a and b show the XRD patterns of Cu-doped Bi_2Te_3 thin films as a function of Cu contents and deposition temperatures. All major peaks were indexed to Bi_2Te_3 (JCPDS no. 15-0863). First in ACu-films, the satellite peaks of Bi_4Te_3 (JCPDS no. 33-0216), BiTe (JCPDS no. 75-1095), and Cu_xTe (JCPDS no. 49-1411) were detected in the range of 21°–35° (Fig. 1c). Cu_xTe phase was observed at the sample with high content of Cu (ACu-7.7), while BiTe and Bi_4Te_3 were formed all ACu-films. The reason for a formation of 2nd phases (BiTe and Bi_4Te_3) is ascribed to the evaporation of Te atoms during a 300 °C aging process after sputtering of the ACu-films. If Cu atoms are heavily doped, like the ACu-7.7 case, excess Cu may form Cu_xTe phase during the thermal annealing [26–28].

Fig. 1e and f present narrow XPS spectra of Te $3d_{3/2}$ in ACu- and HCu-films, respectively. In a Cu-doped Bi_2Te_3 case, the bonding that can be generated are Cu–Te (583.67 eV) [29], Te–Te (583.49 eV) [30], and Bi–Te (582.3 eV) [31,32]. The peak positions of Te $3d_{3/2}$ were 582.6, 582.5, 582.3, and 582.8 eV in ACu-0.0, ACu-0.2, ACu-0.8, and ACu-7.7, respectively. This result informs that Bi_2Te_3 phases were formed, that is well consistent with the result of XRD (Fig. 1).

The additional bonding between Te–Te was found at about 583.7 eV in ACu-0.0, indicating that metallic Te existed in the films [30]. When Te-based chalcogenide thin films such as Sb_2Te_3 [33] and Bi_2Te_3 [22,23] deposited at room temperature were annealed, the segregation of Te can be formed by the evaporation of Te due to its high vapor pressure. The bonding of metallic Te was disappeared at ACu-0.2 and ACu-0.8, and formed again at ACu-7.7 (Fig. 2c). In addition, the value of binding energies of Te $3d_{3/2}$ was slightly decreased as a function of the increase of Cu contents. This tendency was also observed at HCu-films (Fig. 2d), which is related to the effect of Cu doping.

The formation of Bi_2Te_3 crystal structures in the ACu films (ACu-0.0–ACu-7.7) is noteworthy (Fig. 1a) because nearly 50% of Te was determined to be lost (V_{Te}^{2+}) in the annealing process (300 °C) as shown in Table 1. Later in this paper, we will discuss this notable result from the view-point of different major point defects created in between the ACu- and HCu-films (Bi_{Te}^{-}, Cu_{Te}^{2-} *vs.* Cu_{vdW}).

The lattice parameters *c* of ACu- and HCu-films were calculated in Fig. 2a and we tried to discuss the origin of different lattice parameter c between the two deposition processes. The lattice parameter *c* of the ACu-0.2 film (30.496 Å) is bigger than the non-Cu, ACu-0.0 (30.468 Å) film. This increase is confirmed by comparing the parameter *c* of the ACu-0.2 film (30.496 Å) to the reported parameter c (30.284 Å) of an undoped film [32]. Bi_2Te_3 has a hexagonal crystal structure, which is consist of the sequence of $Te^{(1)}$-Bi-$Te^{(2)}$-Bi-$Te^{(1)}$ [12]. In particular, the gap between $Te^{(1)}$ and $Te^{(1)}$ is bonded with weak van der Waals (vdW) force (Fig. 2b) [3,12]. When Cu content was more increased, however, the lattice parameter c was sharply decreased at ACu-0.8 (30.406 nm) and ACu-7.7 (30.397 nm) which is considered to be related with segregation of secondary phases [34]. Different results were observed in HCu-films. The values of HCu-films: HCu-2.7 (29.874 Å), HCu-6.7 (27.758 Å), and HCu-8.1 (29.900 Å) were mostly smaller than those of ACu-films.

In addition, there is another dissimilar XRD result between the ACu- and the HCu-films. The intensity of the peak of (015) crystalline plane are relatively higher than other peaks in ACu-films (Fig. 1a), but not in HCu-films (Fig. 1b). When Sb_2Te_3 or Bi_2Te_3 phases were deposited at room-temperature, the peaks of (015) crystalline plane were mainly dominant in common [25,26,28,33]. In case of the HCu-films, several crystalline planes were formed because sufficient activation energy for moving ad-atoms in the surface of thin films is allowed during deposition [35,36]. SEM analysis represents the difference of microstructure between an ACu-film and a HCu-

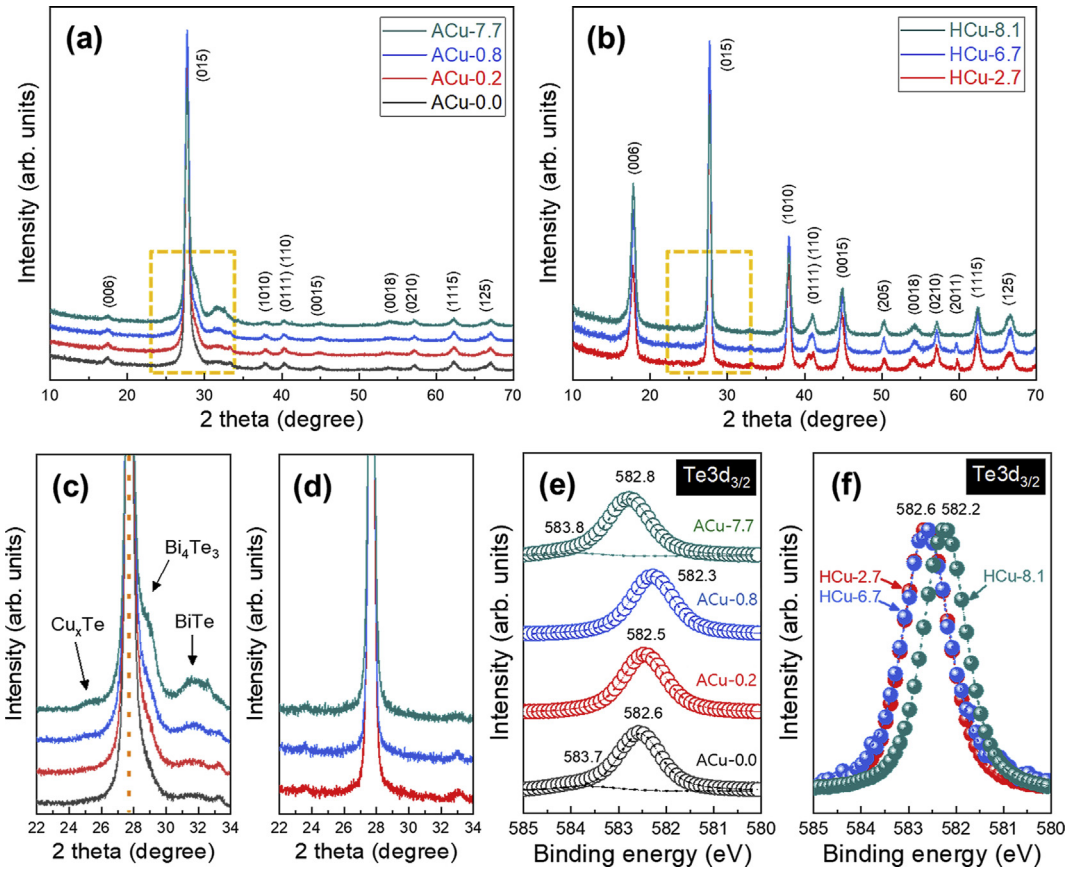

Fig. 1 – XRD patterns of (a) and (c) ACu- and (b) and (d) HCu-films. XPS spectra of (e) ACu- and (f) HCu-films.

film. Fig. 2c shows the anisotropic microstructure of the ACu-film, which is matched to the XRD result representing the remarkably higher peak of (015) crystalline plane than other peaks. On the other hand, Fig. 2d indicates relatively isotropic characteristics of the HCu-film and is also well matched to the relatively isotropic XRD result.

Even though the HCu-films represent relatively more isotropic microstructures than the ACu-films, the anisotropic characteristics of the HCu-films are also detected to be developed in proportion to Cu-content. The Cu-content dependence of anisotropic microstructure of the HCu-films is ascribed to an amount of a point defect generated and the

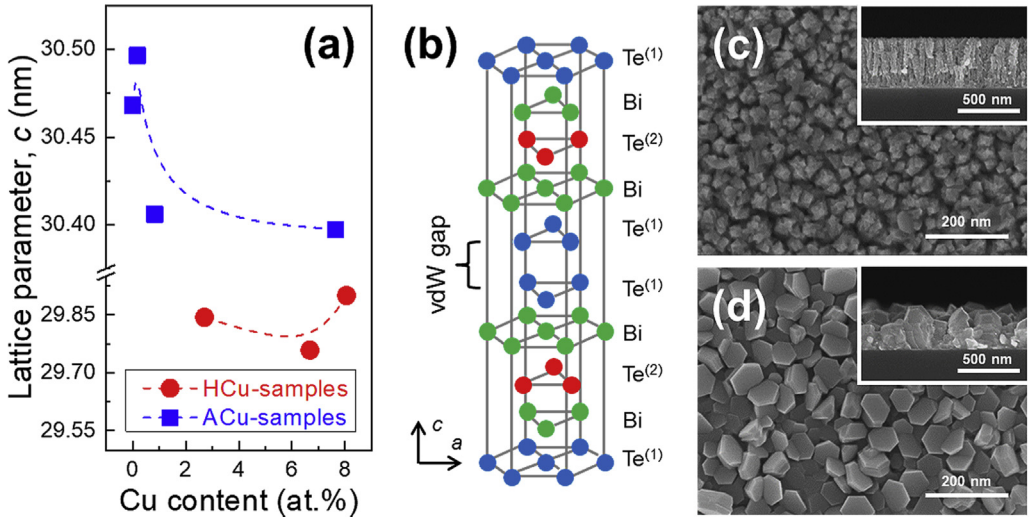

Fig. 2 – (a) Lattice parameters of ACu- and HCu-films as a function of Cu contents. (b) Crystal structure of Bi_2Te_3. Surface-FESEM images of (c) ACu-7.7 and (d) HCu-8.1 films. Insets are cross-sectional FESEM images.

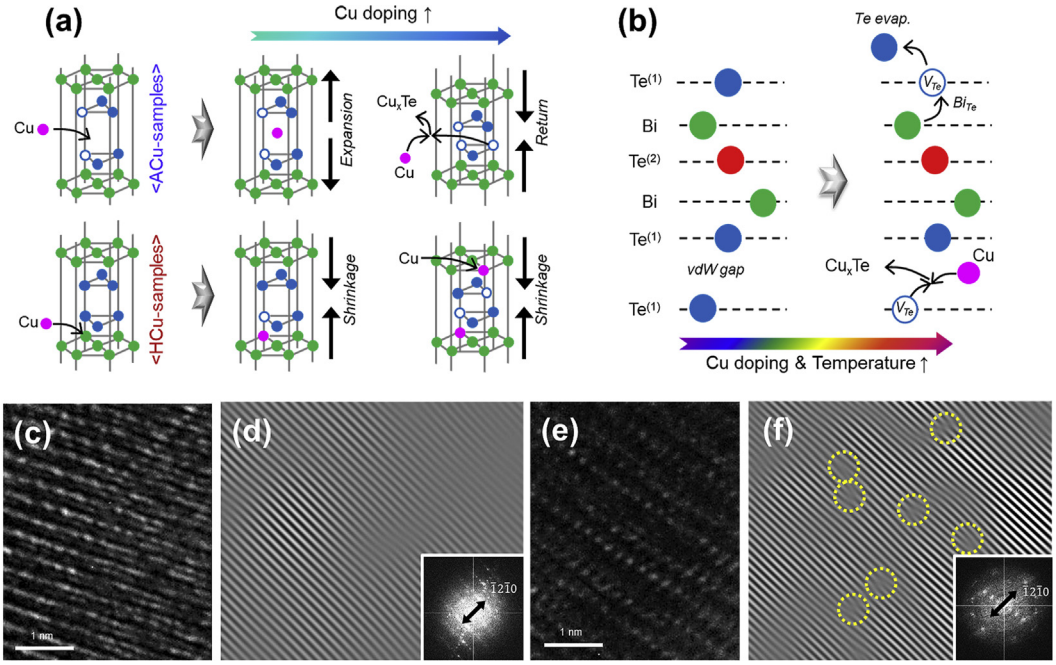

Fig. 3 – Schematics showing, (a) the different behaviors of Cu atoms in ACu- and HCu-films, and (b) the atomic rearrangement in ACu-films. The results of TEM analyses in of ACu-film: (c) HR-TEM images, (d) IFFT pattern obtained from (1210) reflections. The results of TEM analyses in of HCu-film: (e) high-resolution TEM images; (f) IFFT pattern obtained from (1210) reflections.

formation of point defects in these systems will be discussed in detail later.

The XPS and XRD results (Table 1, Figs. 1 and 2) can be summarized in three sentences: (1) We can induce different Te-vacancy (V_{Te}^{2+}) concentrations into the Bi_2Te_3 thin films by using dissimilar deposition processes (ACu- and HCu-) in Cu doped system; (2) Because nearly 50% of Te was determined to be lost in the annealing process (300 °C), it is notable that the ACu-films form a Bi_2Te_3 crystal structure (Bi:Te = 2:3) with a few secondary phases; (3) C-axis lattice parameters increased in ACu-films even with the high Te-vacancy concentration, while those values in HCu-films were smaller than in the ACu-cases.

A Te evaporation in a Bi_2Te_3 material induces a formation of an antisite defect (Bi_{Te}^{-}) by Eqs (1) and (2) [12–14,37,38],

$$Bi_2Te_3 = 2Bi_{Bi}^{\times} + (3-x)Te_{Te}^{\times} + xTe(g)\uparrow + xV_{Te}^{2+} + 2xe^{-} \quad (1)$$

$$\frac{2}{5}xBi_{Bi}^{\times} + xV_{Te}^{2+} + 2xe^{-} = \left(\frac{2}{5}xV_{Bi}^{3-} + \frac{3}{5}xV_{Te}^{2+}\right)^{\times} + \frac{2}{5}xBi_{Te}^{-} + \frac{2}{5}xh^{+} \quad (2)$$

Scherrer et al. reported, the computations on the electronic structure of the defects show that the majority defects present in Bi_2Te_3 are the antisite defects [38]. As shown in Eq. (2), much Te-evaporation (V_{Te}^{2+}) in the ACu-films can accelerate the antisite defect (Bi_{Te}^{-}) formation Eq. (2). The antisite defect (Bi_{Te}^{-}) concentration in the ACu-films is considered to be much higher than the HCu-films. The formation of lots of antisite defect (Bi_{Te}^{-}) can explain why the ACu-films maintain the Bi_2Te_3 crystal structure (Bi:Te = 2:3) even with large amount (2:1.4 ~ 2:1.7) of the Te-deficient (V_{Te}^{2+}). The antisite defect (Bi_{Te}^{-}) is usually reported in Bi_2Te_3 materials because of the small difference in the electronegativity (Bi 1.8, Te 2.1) and in atomic size (Bi 1.60 Å and Te 1.40 Å) [41]. A Cu dopant in Bi_2Te_3 film generally makes a Cu_{Bi}^{2-} defect by an Eq. (3) [12].

$$2Bi + 3Te + xCu_{addition} \rightarrow 2Bi_{Bi}^{\times} + 3Te_{Te}^{\times} + xCu_{Bi}^{2-} + \frac{3}{2}xV_{Te}^{2+} + xe^{-} \quad (3)$$

As shown in Eq. (3) the high Te vacancy (V_{Te}^{2+}) concentration in ACu-films can accelerate the inverse reaction rate of the Eq. (3), which may inhibit the formation of a Cu_{Bi}^{2-} defect [12].

In turn, many research groups reported a small expansion of lattice parameter *c* in Cu doped into Bi_2Te_3 systems. This expansion is ascribed to the intercalation of Cu atoms into the gap of van der Waals [12,39]. The formation of the Cu_{vdW} defect could be an evidence for a restricted Cu_{Bi}^{2-}-formation by the high Te-vacancy (V_{Te}^{2+}) concentration as expressed in the Eq. (3). Therefore, the lattice parameter c increments in ACu-films are also ascribed to the high Te-vacancy concentration in the ACu-films.

In turn, the Cu_{Bi}^{2-}-defects in the HCu-films may be relatively higher than the ACu-films because of the low Te vacancy (V_{Te}^{2+}) concentration. When a foreign atom is substituted for a matrix material, the shrinkage of a crystal structure can be occurred if the size of the doping atom is smaller than that of the composite atoms in matrix. The atomic size of Cu is 0.135 nm [40], while that of Bi is 0.160 nm [40]. The lattice parameter c decrement in the HCu-films seems to be owing to the Cu_{Bi}^{2-} defects produced in HCu-films because of low the Te-vacancy (V_{Te}^{2+}) concentration as mentioned above in Eq. (3). Another reason for the smaller lattice parameter *c* of the HCu-

films may be lower level of the antisite defect (Bi_{Te}^{-}) concentration in the HCu-films than the ACu-films since the Bi 0.160 nm has larger atomic radius than Te 0.140 nm [38,40].

The reason for sharp decrement in the lattice parameter *c* at ACu-0.8 (30.406 nm) and ACu-7.7 (30.397 nm) may be due to an intercalation limit of Cu atoms in the gap of van der Waals, which is reported to under 5 % [27,39]. Cu atoms added over the limit ascribed to produce a Cu_2Te phase as a 2nd phase. As mentioned above in Fig. 1, no secondary phases were formed in HCu-samples, while the 2nd phases were detected in ACu-films. We described this may also be due to the relatively high crystallization rate of HCu-films, which was originated from different preparation processes of ACu- and HCu-films. In case of ACu-films, the reaction among composition atoms cannot easily be occurred during rearrangement of atoms (or clusters).

Figs. 3a and b present different defects formations (Cu_{Bi}^{2-}, Bi_{Te}^{-}, Cu_{vdW}) between the ACu- and HCu-films with distinguished Te-vacancy (V_{Te}^{2+}) concentrations. Fig. 3a schematically represents reason why the lattice parameters between the HCu-films and the ACu-films showed different tendency. Fig. 3b indicates the effect of the Te-vacancy (V_{Te}^{2+}) which made the Cu-additive form a Cu-intercalation into a van der Waals layer (a Cu_{vdW} defect). We presented the TEM analysis results from both films in the Fig. 3c-d of ACu-films and Fig. 3e-f of HCu-films. Dense dislocations (dotted yellow circles) were observed at IFFT pattern in HCu films (Figs. 3e-f), while not in ACu films (Figs. 3c-d). The result is considered to be mainly due to the different Cu (Cu_{Bi}^{2+}) concentrations between the films made by dissimilar sputtering processes. They could also induce a difference in thermoelectric properties between the films. More detailed research for defect structure in this system should be proceeded as a follow-up.

Fig. 4a shows that the electrical conductivities of ACu-films were lower than those of HCu-films. Generally, an electrical conductivity depends on the carrier concentration and the carrier mobility. As mentioned above, large amount of antisite defects (Bi_{Te}^{-}) can be created in the ACu-films. So, an electron concentration in the ACu-films is thought to be lower than the HCu-cases because an antisite defect can act as an acceptor as described in Eq. (2) [7]. The low electron concentration owing to the antisite defect (Bi_{Te}^{-}) formation was confirmed by the larger Seebeck coefficients of the ACu-films than the HCu-films as shown in Fig. 4b.

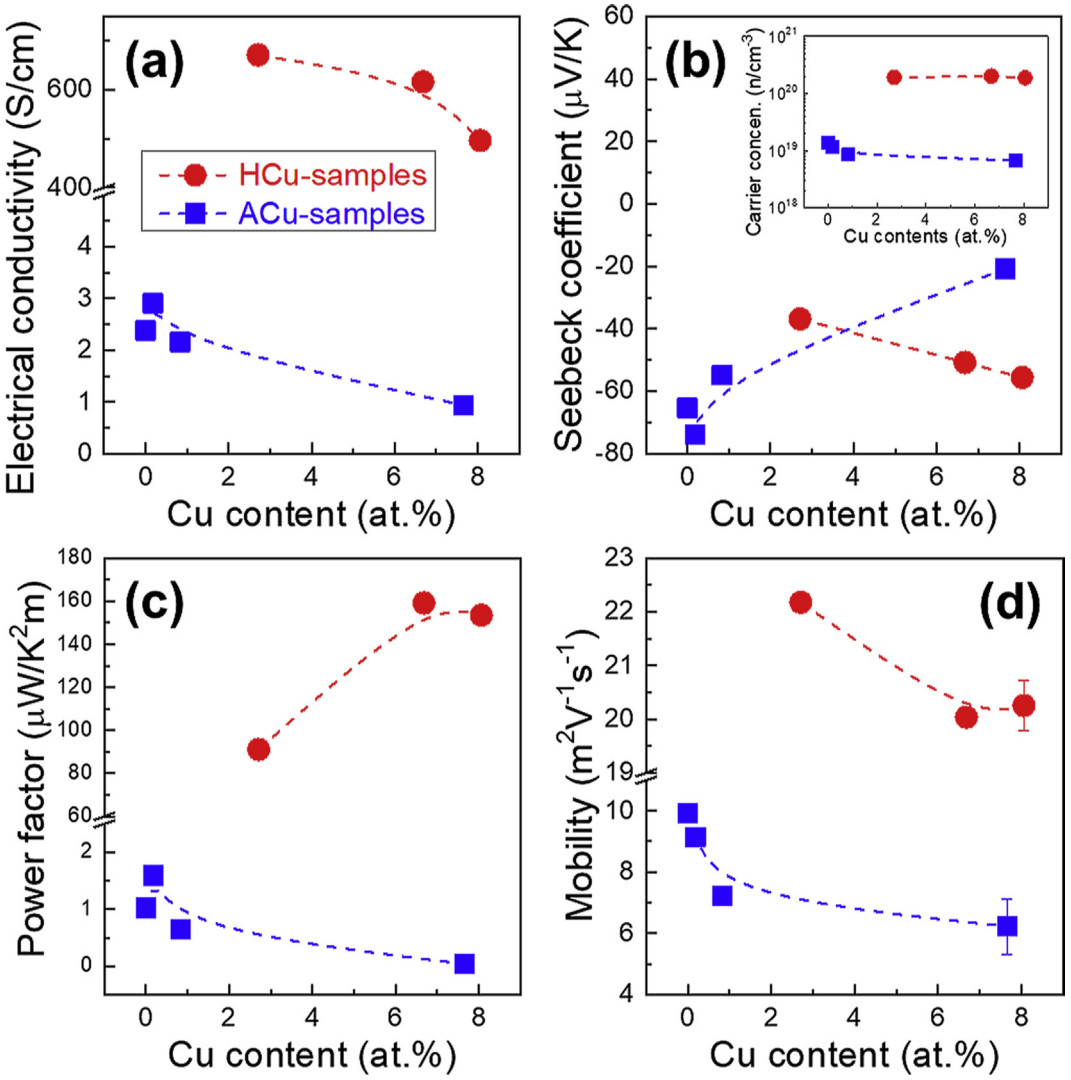

Fig. 4 – (a) Electrical conductivities, (b) Seebeck coefficients, (c) mobilities, and (d) power factors of ACu- and HCu-films. The inset in Fig. 4(b) is the carrier concentrations of ACu- and HCu-films.

Fig. 4c compared the carrier mobility of the two systems, which is influenced by the morphological difference, crystal size, and crystal orientation. The influence of crystal size as a function of Cu contents is ignored in all films because it is very similar to each other (Supporting Information S1). In case of ACu-films, in addition to this, secondary phases ($Cu_{1-x}Te_x$, Te-deficient Bi_2Te_{3-x}) also acted as obstacles for proceeding of electrons [4,27,41]. The electrical conductivities of all the samples were gradually decreased with increase of Cu content except for ACu-0.2. This may be due to the distortion of Bi_2Te_3 crystalline structure and the formation of secondary phases. Power factor values from the two types of films were compared in the Fig. 4d. Those of the HCu-films were much higher than the values of the ACu-films, which are ascribed to higher carrier concentration and higher mobility than those of the ACu-cases.

4. Conclusions

In summary, two different sputtering processes produced Cu-doped Bi_2Te_3 thin films with different concentrations of Te-vacancies (V_{Te}^{2+}). The Cu-doped Bi_2Te_3 films with a low Te-vacancy concentration (V_{Te}^{2+}) were made by a high temperature deposition process at 200 °C, in which the Cu additives were successfully substituted for Bi-sites (Cu_{Bi}^{2-}). The high electronic concentration and the low Seebeck coefficient were also considered as the evidences for the low Te-vacancy concentration (V_{Te}^{2+}).

The Cu-doped Bi_2Te_3 films with high V_{Te}^{2+}-defect concentrations were fabricated from a two-step sputter process: a deposition at room temperature and a followed annealing at 300 °C. In this case the high V_{Te}^{2+}-defect concentrations inhibited a Cu_{Bi}^{2-}-formation reaction. The Cu-additive was considered to produce a Cu-intercalation into a van der Waals layer (a Cu_{vdW} defect). We detected an increased lattice parameter as an evidence for the Cu-intercalation (Cu_{vdW}) of the Cu additives. For the case of high V_{Te}^{2+}-defect concentration, the Te-vacancy (V_{Te}^{2+}) was charge compensated by an antisite defect (Bi_{Te}^{-}). The lower electrical conductivity, and the higher Seebeck coefficient were considered as evidences for the formation of the Bi_{Te}^{-} defect acted as an acceptor. The different Te-vacancy (V_{Te}^{2+}) concentrations from dissimilar deposition steps were a decisive parameter for crystal structure and thermoelectric property in the Cu-doped Bi_2Te_3 films.

Declaration of Competing Interest

The authors declare that they have no known competing financial interests or personal relationships that could have appeared to influence the work reported in this paper.

Acknowledgment

This research was supported by the Basic Science Research Program (NRF-2017R1D1A1A09000570). This research was also supported by Basic Science Research Program through the National Research Foundation of Korea funded by the Ministry of Education (No. NRF-2018R1D1A1A02086218).

Appendix A. Supplementary data

Supplementary data to this article can be found online at https://doi.org/10.1016/j.jmrt.2021.07.147.

REFERENCES

[1] Goldsmith HJ. Theory of thermoelectric devices. In: Applications of thermoelectricity. London: Methuen & Co Ltd; 1960. Chap. 2.
[2] Rowe DM. General principles and basic consideration. In: Rowe DM, editor. Thermoelectrics handbook: macro to nano. Boca Raton, FL: Taylor & Francis; 2006. Chap. 1.
[3] Goldsmith HJ. Conversion efficiency and figure-of-merit. In: Rowe DM, editor. CRC handbook of thermoelectrics: macro to Nano. Boca Raton, FL: CRC Press; 1995. Chap. 3.
[4] Kim SI, et al. Dense dislocation arrays embedded in grain boundaries for high-performance bulk thermoelectrics. Science 2015;348:109.
[5] Madar N, et al. High thermoelectric potential of Bi_2Te_3 alloyed GeTe- rich phases. J Appl Phys 2016;120:035102.
[6] Sadia Y, et al. Criteria for extending the operation periods of thermoelectric converters based on IV-VI compounds. J Solid State Chem 2016;241:79–85.
[7] Ben-Ayoun D, et al. High temperature thermoelectric properties evolution of $Pb_{1-x}Sn_xTe$ based alloys. J Alloys Compd 2017;722:33–8.
[8] Meroz O, et al. Development of $Bi_2Te_{2.4}Se_{0.6}$ alloy for thermoelectric power generation applications. J Alloys Compd 2016;679:196–201.
[9] Sadia Y, et al. Thermoelectric properties in the quasi-binary $MnSi_{1.73}$-$FeSi_2$ system. J Electron Mater 2015;44:1637.
[10] Poudel B, et al. High-thermoelectric performance of nanostructured bismuth antimony telluride bulk alloys. Science 2008;320:634.
[11] Ma Y, et al. Enhanced thermoelectric figure-of-merit in p-type nanostructured bismuth antimony tellurium alloys made from elemental chunks. Nano Lett 2008;8:2581.
[12] Liu W-S, et al. Thermoelectric property studies on Cu-doped n-type $Cu_xBi_2Te_{2.7}Se_{0.3}$ nanocomposites. Adv. Energy Mater. 2011;1:577.
[13] Horak J, Navartils J, Stary Z. Lattice point defects and free-carrier concentration in $Bi_{2+x}Te_3$ and $Bi_{2+x}Se_3$ crystals. J Phys Chem Solid 1992;53:1067.
[14] Scanlon DO, et al. Controlling bulk conductivity in topological insulators: key role of anti-site defects. Adv Mater 2012;24:2154.
[15] Tan, et al. Synergistically optimized thermoelectric performance in $Bi_{0.48}Sb_{1.52}Te_3$ by hot deformation and Cu doping. ACS Appl Energy Mater 2019;2:6714–9.
[16] Kim, et al. Stress-induced change of Cu-doped Bi_2Te_3 thin films for flexible thermoelectric applications. Mater Lett 2020;270:127697.
[17] Padmanathan, et al. Amorphous framework in electrodeposited CuBiTe thermoelectric thin films with high room-temperature performance. ACS Appl. Electron. Mater. 2021;3:1794–803.
[18] Goldsmid HJ. Recent studies of bismuth telluride and its alloys. J Appl Phys 1961;32:2198.
[19] Wuttig M, et al. Phase-change materials for rewritable data storage. Nat Mater 2007;6:824.

[20] Kolobov AV, et al. Understanding the phase-change mechanism of rewritable optical media. Nat Mater 2004;3:703.
[21] Wang X, et al. Effects of annealing temperature on thermoelectric properties of Bi_2Te_3 films prepared by co-sputtering. Appl Surf Sci 2013;276:539.
[22] Huang H, et al. Influence of annealing on thermoelectric properties of bismuth telluride films grown via radio frequency magnetron sputtering. Thin Solid Films 2009;517:3731.
[23] Zhang Y, et al. Characteristics of Si-doped Sb_2Te_3 thin films for phase-change random access memory. Appl Surf Sci 2008;254:5602.
[24] Kim BG, et al. Free-standing Bi–Sb–Te films derived from thermal annealing of sputter-deposited Sb_2Te_3/Bi_2Te_3 multilayer films for thermoelectric applications. CrystEngComm 2015;17:7522.
[25] Kim D-H, et al. Effect of deposition temperature on the structural and thermoelectric properties of bismuth telluride thin films grown by co-sputtering. Thin Solid Films 2016;510:148.
[26] Seo KH, et al. Doping amount dependence of phase formation and microstructure evolution in heavily Cu-doped Bi_2Te_3 films for thermoelectric applications. CrystEngComm 2017;19:2750.
[27] Wang Z-L, et al. Effect of Cu doping on microstructure and thermoelectric properties of $Bi_2Te_{2.85}Se_{0.15}$ bulk materials. Scripta Mater 2018;146:119.
[28] Mun H, et al. Boundary engineering for the thermoelectric performance of bulk alloys based on bismuth telluride. ChemSusChem 2015;8:2312.
[29] Nethravathi C, et al. Synthesis and thermoelectric behaviour of copper telluride nanosheets. J Mater Chem A 2014;2:985.
[30] Moulder JF, et al. Handbook of X-ray photoelectron spectroscopy. Chanhassen: Physical Electronics, Inc.; 1991.
[31] Liu N, et al. Conducting mechanism of Ag-diffused Bi–Te based resistive switching devices. Appl Phys A 2018;124:143.
[32] Guo JH, et al. Surface oxidation properties in a topological insulator Bi_2Te_3 film. Chin Phys Lett 2013;30:106801.
[33] Kim BG, et al. Control of selective and catalyst-free growth of Sb_2Te_3 and Te nanowires from sputter-deposited Al-Sb-Te thin films. CrystEngComm 2012;14:4255.
[34] Li, et al. Synthesis of highly b-oriented zeolite MFI films by suppressing twin crystal growth during the secondary growth. CrystEngComm 2011;13:3657.
[35] Zhang P, et al. A computer simulation of nucleation and growth of thin films. Comput Mater Sci 2004;30:331–6.
[36] Galdikas A. Non-monotonous dependence of surface roughness on factors influencing energy of adatoms during thin island film growth. Surf Sci 2006;600:2705–10.
[37] Chitroub M, et al. Anisotropy of the selenium diffusion coefficient in bismuth telluride. J Phys Chem Solid 2000;61:1693.
[38] Oh MW, et al. Antisite defects in n-type $Bi_2(Te,Se)_3$: experimental and theoretical studies. J Appl Phys 2014;115:133706.
[39] Sie FR, et al. Thermoelectric performance of n-type Bi_2Te_3/Cu composites fabricated by nanoparticle decoration and spark plasma sintering. J Electron Mater 2016;45:1927.
[40] Slater JC. Atomic radii in crystals. J Chem Phys 1964;41:3199.
[41] Kim W. Strategies for engineering phonon transport in thermoelectrics. J Mater Chem C 2015;3:10336.